

# Current Biology

## Distinct Circuits for Recovery of Eye Dominance and Acuity in Murine Amblyopia

### Highlights

- Recovery of eye dominance and acuity are independent in murine amblyopia
- *ngr1* operates in neocortex to limit recovery of eye dominance
- *ngr1* expression by thalamic neurons restricts improvement of acuity
- Deleting *ngr1* after the critical period is sufficient to restore acuity

### Authors

Céleste-Élise Stephany,  
Xiaokuang Ma, Hilary M. Dorton, ...,  
Michael G. Frantz, Shenfeng Qiu,  
Aaron W. McGee

### Correspondence

squiu@email.arizona.edu (S.Q.),  
aaron.mcgee@louisville.edu (A.W.M.)

### In Brief

Early visual deprivation yields enduring deficits in both eye dominance and acuity. Stephany et al. demonstrate that *ngr1* limits restoration of eye dominance and acuity within distinct components of visual circuitry to reveal that recovery of these facets of vision is independent in a murine model of amblyopia.

# Distinct Circuits for Recovery of Eye Dominance and Acuity in Murine Amblyopia

Céleste-Élise Stephany,<sup>1,2</sup> Xiaokuang Ma,<sup>3,4</sup> Hilary M. Dorton,<sup>1,2</sup> Jie Wu,<sup>4,5,6</sup> Alexander M. Solomon,<sup>1,2</sup> Michael G. Frantz,<sup>1,2</sup> Shenfeng Qiu,<sup>3,4,\*</sup> and Aaron W. McGee<sup>1,2,6,7,\*</sup>

<sup>1</sup>Developmental Neuroscience Program, Saban Research Institute, Children's Hospital Los Angeles, Los Angeles, CA 90027, USA

<sup>2</sup>Department of Pediatrics, Keck School of Medicine, University of Southern California, Los Angeles, CA 90027, USA

<sup>3</sup>Department of Basic Medical Sciences, University of Arizona College of Medicine-Phoenix, Phoenix, AZ 85004, USA

<sup>4</sup>Department of Physiology, Shantou University Medical College, Shantou, 515041 Guangdong, China

<sup>5</sup>Departments of Neurology and Neurobiology, Barrow Neurological Institute, St. Joseph's Hospital and Medical Center, Phoenix, AZ 85013, USA

<sup>6</sup>Department of Anatomical Sciences and Neurobiology, University of Louisville, Louisville, KY 40202, USA

<sup>7</sup>Lead Contact

\*Correspondence: [sqiu@email.arizona.edu](mailto:sqiu@email.arizona.edu) (S.Q.), [aaron.mcgee@louisville.edu](mailto:aaron.mcgee@louisville.edu) (A.W.M.)

<https://doi.org/10.1016/j.cub.2018.04.055>

## SUMMARY

Degrading vision by one eye during a developmental critical period yields enduring deficits in both eye dominance and visual acuity. A predominant model is that “reactivating” ocular dominance (OD) plasticity after the critical period is required to improve acuity in amblyopic adults. However, here we demonstrate that plasticity of eye dominance and acuity are independent and restricted by the *nogo-66 receptor (ngr1)* in distinct neuronal populations. *Ngr1* mutant mice display greater excitatory synaptic input onto both inhibitory and excitatory neurons with restoration of normal vision. Deleting *ngr1* in excitatory cortical neurons permits recovery of eye dominance but not acuity. Reciprocally, deleting *ngr1* in thalamus is insufficient to rectify eye dominance but yields improvement of acuity to normal. Abolishing *ngr1* expression in adult mice also promotes recovery of acuity. Together, these findings challenge the notion that mechanisms for OD plasticity contribute to the alterations in circuitry that restore acuity in amblyopia.

## INTRODUCTION

Experience has a prominent role in sculpting brain circuitry during development, yet experience-dependent plasticity diminishes with age. Amblyopia exemplifies how reduced neural plasticity in adulthood impairs recovery from maladaptive alterations to brain circuitry arising during development. This prevalent childhood disorder is caused by discordant vision and results in a number of deficits in spatial vision including lower acuity [1]. Associated visual impairments are largely permanent if untreated before the closure of a “critical period” that ends in adolescence. Although some therapeutic approaches have reported improvements in acuity in older patients [2], the critical period confines both the age of sensitivity to discordant vision as well as the opportunity for effective treatment.

The predominant model for the pathophysiology of amblyopia is that discordant vision exaggerates eye dominance and thereby limits processing of visual information from the affected eye and lowers visual performance. These maladaptive changes within visual circuitry are then consolidated with the closure of the critical period. Consistent with this model, perturbing vision through one eye by lid suture also yields enduring impairments in eye dominance and visual acuity in numerous mammals with binocular vision [3]. Although significant efforts have been put forth to understand the neurological basis of amblyopia, determining the relationship between abnormal eye dominance and low acuity has proven challenging.

Anatomical and physiological properties of cells in the retina, lateral geniculate nucleus (LGN), and visual cortex have been examined to understand how amblyopia changes the spatial organization and function of neurons within visual circuitry. Overall, there is consensus that amblyopia results in few permanent deficits in the retina (e.g., [4]). Whether amblyopia-induced changes to the relay neurons in LGN contribute to the observed deficits in visual acuity remains controversial (see Discussion). Primary visual cortex (V1) is considered a locus of amblyopia because of the loss of binocular responses following visual deprivation during the critical period [5].

Amblyopia can be induced in rodents by depriving one eye of vision for the duration of the critical period (long-term monocular deprivation [LTMD]). LTMD drives a persistent shift in ocular dominance toward the non-deprived eye as measured by extracellular electrophysiological recordings in V1 [6–8]. This diminished representation of the deprived eye in V1 is accompanied by a modest reduction in the distribution of thalamocortical axons subserving this eye [8]. LTMD also permanently decreases visual acuity of the previously deprived eye. One direct approach for measuring acuity in mice and rats is a behavioral assay assessing visually guided performance, the visual water task (VWT) [9].

Mice constitutively lacking the gene for the neuronal *nogo-66 receptor 1 (ngr1-/-)* recover visual acuity following LTMD after 7 weeks of normal vision as measured with this task [10]. To date, *ngr1* is the only gene yet implicated as limiting recovery of visually guided performance. The protein product of the *ngr1* gene

(NgR1) is a leucine-rich repeat protein that is attached to the outer leaflet of the plasma membrane of neurons by a glycosyl-phosphatidylinositol (GPI) anchor. NgR1 has been reported to localize both to axons as well as dendrites and dendritic spines [11, 12] and is expressed in retina, LGN, and V1 [13, 14]. NgR1 is a receptor for several disparate extracellular ligands associated with myelin and perineuronal nets implicated in restricting anatomical and synaptic plasticity [15, 16].

Previously, we generated a conditional allele of *ngr1* (*ngr1<sup>fl/fl</sup>*) [17]. Deleting *ngr1* in parvalbumin-positive (PV) interneurons prevents the closure of the critical period for ocular dominance (OD) plasticity. This sustained OD plasticity is accompanied by the capacity for short durations (1 or 2 days) of monocular deprivation (MD) to promote disinhibition within the intracortical circuitry of V1 [10, 18]. However, deleting *ngr1* in PV interneurons is not sufficient to improve acuity following LTMD [18]. Thus, OD plasticity observed with 4-day MD could be necessary but not sufficient for recovery of acuity, or OD plasticity and acuity could be independent.

Here, we combine this conditional *ngr1* allele with brain-region- and cell-class-specific Cre drivers to dissect where within the circuitry of the visual system plasticity is required to restore eye dominance and improve acuity in the murine model of amblyopia. We measure plasticity with electrophysiological recordings *in vivo*, circuit mapping in visual cortex by laser-scanning photostimulation, and the behavioral assay of visual acuity. Unexpectedly, we discover that whereas *ngr1* operates within excitatory cortical neurons to limit the recovery of eye dominance following LTMD, improvement of visual acuity is independently governed by *ngr1* expression in thalamus. We propose that alterations in circuitry sufficient to improve acuity in amblyopia do not require OD plasticity and identify subcortical circuitry as a target for therapeutic intervention.

## RESULTS

### Recovery of Normal Eye Dominance Is Preceded by Increased Excitatory Synaptic Input to Both Inhibitory and Excitatory Neurons in Visual Cortex

LTMD initiated early in the critical period (~postnatal day 24 [P24]) induces a permanent OD shift toward the non-deprived eye [7]. Mice lacking *ngr1* display both normal eye dominance biased to the contralateral eye and sensitivity to LTMD during the critical period. However, *ngr1* mutant mice partially recover contralateral bias within 8 days of restoration of binocular vision following LTMD [19]. To determine whether a prolonged duration of binocular vision would yield a more complete recovery of normal eye dominance in *ngr1*(*-/-*) mice, we permitted 7 weeks of binocular vision following LTMD before performing extracellular electrophysiological recordings to measure OD in wild-type (WT) and *ngr1*(*-/-*) mice (Figure 1A).

Following 7 weeks of binocular vision, abnormal eye dominance is sustained in WT mice. WT mice exhibited a rightward shift in the OD histograms (Figure S1; related to Figure 1), a significant decrease in the median contralateral bias index (CBI) score (Figure 1B; WT versus WT LTMD  $p = 0.005$ ; Kruskal-Wallis [KW] test for multiple comparisons), and a rightward shift in the cumulative distribution of OD scores for individual units (Figure 1C;  $p < 0.0001$ , Kolmogorov-Smirnov [K-S] test of cumulative

distribution). In contrast, *ngr1*(*-/-*) mice displayed normal eye dominance with 7 weeks of binocular vision following LTMD. The median CBI score and cumulative distribution of OD scores for individual units was not significantly different than non-deprived mice (Figures 1B and 1C;  $p > 0.9$  CBI WT versus *ngr1*(*-/-*) LTMD;  $p = 0.72$ ; K-S test). To evaluate the time course and magnitude of recovery of eye dominance for WT and *ngr1*(*-/-*) mice, we re-plotted these CBI scores after 7 weeks of binocular vision post-LTMD next to our published CBI scores for WT and *ngr1* mutants after 4 weeks of LTMD and LTMD followed by 8 days of binocular vision (Figure 1D) [19]. The limited recovery of eye dominance observed in WT mice at 8 days after re-opening the eye was sustained but not augmented by 7 weeks post-LTMD. By comparison, recovery of eye dominance by *ngr1*(*-/-*) mice with 8 days of binocular vision was similar to WT mice at 7 weeks and continued to improve, reaching the normal range by 7 weeks. Thus, *ngr1* limits recovery of normal eye dominance guided by restored binocular vision after the critical period.

An early and essential component of OD plasticity during the critical period is intracortical disinhibition [20]. MD occludes sensory input from the closed eye, and this reduced input drives a compensatory weakening of cortical excitatory synapses onto interneurons expressing PV. This disinhibition is proposed to be permissive rather than instructive for subsequent shifts in eye dominance by competitive mechanisms. Recently, we demonstrated that *ngr1* confines this disinhibition following MD to the critical period [18]. To investigate whether the restoration of vision and resulting recovery of eye dominance also engages plasticity within inhibitory circuitry, we examined the strength of excitatory synaptic drive onto PV interneurons in layer (L)2/3 with laser-scanning photostimulation for WT and *ngr1*(*-/-*) mice (Figures 2A–2C).

We compared the strength and distribution of excitatory synaptic currents onto L2/3 PV interneurons after 4 weeks of LTMD (P24–P45) and LTMD followed by one day of binocular vision for WT and *ngr1*(*-/-*) mice (Figures 2 and S2). Re-opening the sutured eye induced a modest but statistically significant increase in the excitatory synaptic input onto L2/3 PV neurons in V1 contralateral to the LTMD in WT mice (WT LTMD  $6.9 \text{ pA} + 1.5$  versus WT LTMD + 1 day  $10.4 \text{ pA} + 1.8$ ;  $p = 0.005$ ; MW test; Figure 2E). By comparison, one day of vision doubled the average synaptic input from L4 in *ngr1*(*-/-*) mice (*ngr1* LTMD  $12.1 \text{ pA} + 1.9$  versus *ngr1* LTMD + 1 day  $23.8 \text{ pA} + 3.2$ ;  $p = 0.0003$ ; MW test; Figure 2E). Eye opening following LTMD did not alter the intrinsic excitability of PV interneurons to current injection for either WT or *ngr1* mutant mice (Figure S2; related to Figure 2) or the excitation profiles to glutamate uncaging (data not shown). Thus, plasticity within inhibitory cortical circuitry also precedes restoration of normal eye dominance with binocular vision following LTMD, but this OD plasticity is accompanied by a strengthening of cortical excitatory synapses onto PV interneurons rather than the weakening associated with brief MD.

To assess whether recovery of eye dominance with restoration of binocular vision was associated with alterations to the synaptic input onto thalamo-recipient L4 pyramidal neurons, we examined the frequency and amplitude of miniature excitatory post-synaptic currents (mEPSCs) after LTMD, LTMD

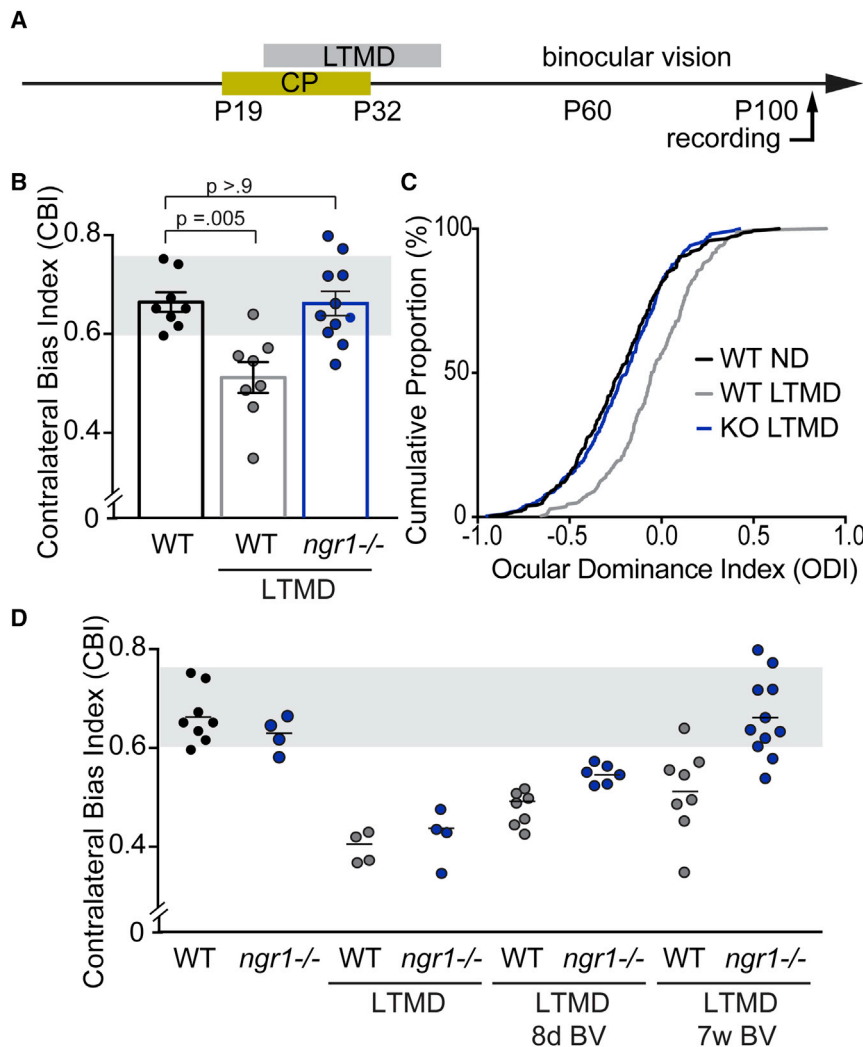


**Figure 1. Recovery Normal Eye Dominance with 7 Weeks of Binocular Vision following LTMD by *ngr1(-/-)* Mice**

(A) Schematic of the timeline for long-term monocular deprivation (LTMD) and period of binocular vision prior to electrophysiologic recording to assess ocular dominance (OD) in adult (P90–P120) *ngr1(-/-)* and WT mice.

(B) CBI scores for non-deprived WT mice ( $n = 8$ ) and WT and *ngr1(-/-)* mice receiving LTMD ( $n = 8$  and 11). Groups receiving LTMD are underlined. Each point represents the CBI for an individual animal, and the bars represent the average for each group with error bars for SEM. The gray box indicates the typical range of CBI scores for non-deprived mice.

(C) Cumulative histograms of OD scores for groups reported in (B) (WT, 288 units; WT LTMD, 248 units; *ngr1(-/-)* LTMD, 336 units).

(D) A comparison of recovery of eye dominance following increasing duration of binocular vision (BV) subsequent to LTMD. CBI scores for WT and *ngr1(-/-)* mice during LTMD and following 8 days of BV were previously published in [19] and are presented here for comparison to 7 weeks after re-opening the closed eye.

Error bars represent  $\pm$  SEM. See also Figure S1.

### Neocortex Limits Recovery of Eye Dominance following LTMD

NgR1 is expressed along the visual pathway in both the LGN of the thalamus as well as visual cortex [13]. To determine where NgR1 operates within visual circuitry to limit the recovery of eye dominance with binocular vision following LTMD, we examined mice possessing a conditional *ngr1* allele (*ngr1(f/f)*) [17]. In this conditional allele, *loxP* sites flank

followed by one day of binocular vision, and LTMD followed by 4 weeks of binocular vision, in both WT and *ngr1(-/-)* mice (Figure 3A). Restoring vision to the closed eye yielded a transient increase in the frequency of mEPSCs in WT mice, as after 4 weeks of binocular vision the frequency of events was significantly lower than after 1 day ( $p = 0.03$ ; KW test; Figure 3B). By comparison, the increase in the frequency of mEPSCs 1 day following re-opening the closed eye was sustained 4 weeks later in *ngr1(-/-)* mice ( $p > 0.9$ ; KW test) and was significantly greater than the frequency of mEPSCs measured in WT mice at 4 weeks subsequent to LTMD ( $p = 0.008$ ; KW test). Cumulative distributions for the amplitudes of mEPSCs from L4 pyramidal neurons were similar for WT and *ngr1(-/-)* mice during LTMD. However, the amplitudes of mEPSCs were significantly greater in *ngr1* mutant mice from 1 day to 4 weeks following eye re-opening ( $p < 0.0001$ ; K-S tests; Figure 3C). The intrinsic excitability of L4 neurons was also indistinguishable between genotypes and deprivation conditions (Figure S3; related to Figure 3). These sustained increases in mEPSC frequency and amplitude correlate with the spontaneous yet slow recovery of eye dominance and acuity in *ngr1(-/-)* mice.

exon 2 that contains the entire protein coding sequence of the mature receptor. In the presence of *Cre* recombinase, the expression of NgR1 is abolished and GFP is expressed from the *ngr1* gene locus (Figure S4; related to Figure 4) [17]. In the absence of *Cre* recombinase, GFP expression is not detectable by immunofluorescence staining of coronal brain sections (Figure 4A).

OD plasticity is generally considered to originate in V1, as it does not require protein synthesis in LGN [21]. However, recent studies have reported some degree of binocularity and OD plasticity in thalamus of both juvenile and adult mice [22–24]. Therefore, we tested whether NgR1 expression in cortex restricts recovery of eye dominance following LTMD. We selectively abolished NgR1 expression in excitatory neurons in cortex and/or LGN by combining the *ngr1* conditional allele with one of three transgenic *Cre* drivers (Figures 4B–4D). We measured eye dominance in each of these lines after 6 weeks of binocular vision following LTMD with electrophysiologic recordings. Similar to WT mice, *ngr1(f/f)* mutants without *Cre*-mediated recombination display a persistent shift in OD toward the non-deprived eye (Figures 4E and 4F;  $p = 0.003$  CBI fix versus fix LTMD; KW test).

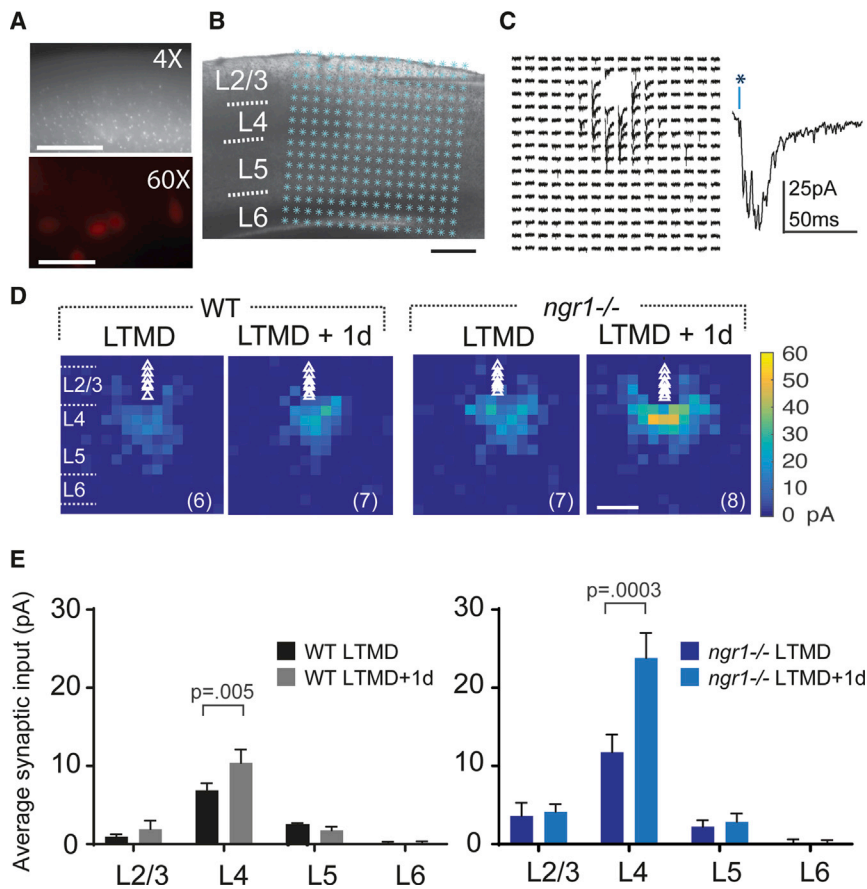


**Figure 2. Recovery of Eye Dominance and Acuity Are Preceded by Elevated Intracortical Excitatory Synaptic Input onto L2/3 PV Interneurons**

(A) Parvalbumin-positive (PV) interneurons identified in both WT and *ngn1(-/-)* mice by tdTomato expression from a Cre-dependent reporter in combination with *PV-Cre*. The scale bars represent 0.5 mm (top) and 50  $\mu$ m (bottom).

(B) Example of a L2/3 PV interneuron recorded in binocular V1 in an acute slice; overlaid are 16  $\times$  16 stimulation locations for laser-scanning photostimulation (LSPS) spanning pia to white matter. The scale bar represents 250  $\mu$ m.

(C) Representative traces from LSPS-evoked EPSCs measured across 16  $\times$  16 locations (75- $\mu$ m spacing) for a L2/3 PV interneuron. Direct somatic responses have been removed for clarity. A higher magnification trace is shown at right.

(D) LSPS aggregate excitatory input maps pooled across PV interneurons for WT and *ngn1(-/-)* mice during LTMD or after 1 day of binocular vision. Triangles indicate soma locations; n = number of cells is in parentheses for each group. The scale bar represents 250  $\mu$ m.

(E) Mean LSPS-evoked EPSC amplitude from neurons recorded in (D) binned into L2/3, L4, L5, and L6. The mean LSPS-evoked amplitudes are greater for both genotypes following 1 day of vision, but the magnitude of the increase is more than double in *ngn1(-/-)* mice. *Ngn1* limits increased excitatory synaptic input onto PV interneurons in visual cortex with restoration of binocular vision.

Error bars represent  $\pm$  SEM. See also Figure S2.

First, we selectively deleted *ngn1* in cortical excitatory neurons with a transgene expressing Cre recombinase under the control of the calcium/calmodulin-dependent protein kinase II alpha (*CamkIIa*) promoter (*CK-Cre*) [25]. *CamkIIa* is expressed in excitatory neurons in forebrain and deletes *ngn1* in cortex but not LGN (Figure 4B). Abolishing *NgR1* expression in cortex was sufficient for recovery of normal contralateral bias with extended binocular vision following LTMD, as the median CBI and the cumulative distribution of OD scores for individual units for *ngn1(f/f);CK-Cre* mice having received LTMD and 6 weeks of normal vision were both similar to non-deprived *ngn1(f/f)* controls (Figures 4E and 4F).

Next, we directed the deletion of *ngn1* to thalamus with two different Cre drivers: *Scnn1a-Cre* and *Olig3-Cre*. *Scnn1a-Cre* drives recombination in thalamus and L4 excitatory cortical neurons (Figure 4C) [26]. Thalamic progenitor cells express the transcription factor *Olig3* [27], and *Olig3-Cre* deletes *ngn1* in thalamus but not neocortex (Figure 4D). After 6 weeks of binocular vision following LTMD, both *ngn1(f/f);Scnn1a-Cre* and *ngn1(f/f);Olig3-Cre* mice retain abnormal eye dominance similar to *ngn1(f/f)* mice. The median CBI scores for both strains were significantly lower than non-deprived *ngn1(f/f)* controls (Figure 4E;  $p = 0.004$  flx versus flx;*Scnn1a-Cre* LTMD;  $p = 0.006$  flx versus flx;*Olig3-Cre* LTMD; KW test). Therefore, abolishing *NgR1* expression in LGN does not permit recovery of normal eye dominance, providing additional evidence that *NgR1* operates in cortex to govern OD plasticity. Furthermore, the limited

recovery of normal contralateral bias in *ngn1(f/f);Scnn1a-Cre* mice reveals that deleting *ngn1* only in L4 is not sufficient to restore normal eye dominance.

In addition, we performed a laminar analysis of OD to evaluate the degree of recovery of eye dominance within each cortical layer. Previously, we reported that the partial recovery of contralateral bias in *ngn1(-/-)* mice can be attributed to plasticity in L2/3 and L5/6. However, this short period of binocular vision does not yield any recovery of OD in L4 [19]. In comparison, after 6 weeks of binocular vision, *ngn1(f/f);CK-Cre* mice had recovered normal eye dominance in L2/3 and L4 and near normal contralateral bias in L5/6 (Figure S5; related to Figure 4), whereas *ngn1(f/f);Scnn1a-Cre* mice, *ngn1(f/f);Olig3-Cre* mice, and *ngn1(f/f)* controls sustained abnormal eye dominance in each layer. Thus, we observe a recovery of normal OD in L4 with 6 weeks of binocular vision in *ngn1(f/f);CK-Cre* that was not evident after 7 days of vision in *ngn1(-/-)* mice [19]. Interestingly, the magnitude of recovery was also largest in L4.

#### Thalamus Restricts Recovery of Visual Acuity following LTMD

To determine where *NgR1* expression is required to limit improvement of visual acuity following LTMD, we tested these combinations of the *ngn1* conditional allele and Cre drivers with the VWT. The VWT is a two-alternative forced-choice task that measures visual acuity [28]. Mice were trained on the task during binocular vision following LTMD, and then we evaluated acuity

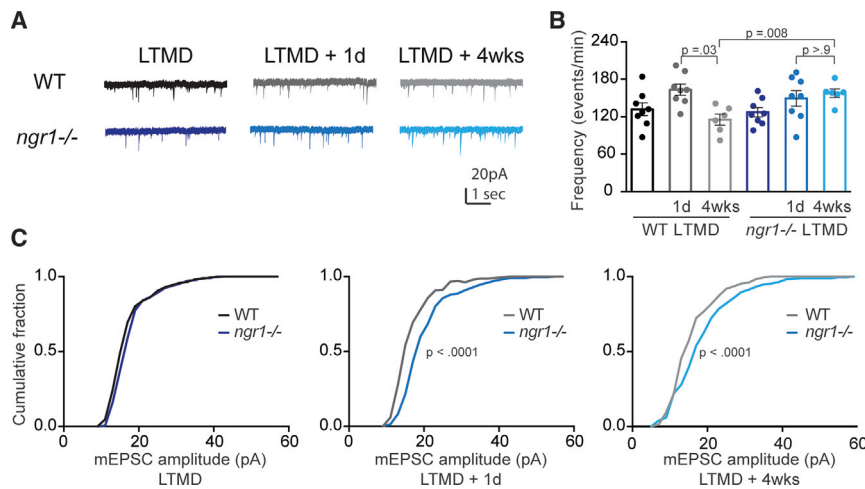


**Figure 3. A Sustained Increase in Excitatory Synaptic Input onto L4 Pyramidal Neurons Precedes Recovery from Visual Deprivation**

(A) Representative traces of spontaneous activity in V1 from acute slices from WT and *ngr1*<sup>-/-</sup> mice during LTMD and LTMD followed by 1 day and 4 weeks of binocular vision.

(B) The frequency of mEPSCs for WT LTMD (n = 8), LTMD + 1 day (n = 8), and LTMD + 4 weeks (n = 6) as well as *ngr1*<sup>-/-</sup> mice in these conditions (n = 8, 8, and 6, respectively). Whereas both WT and *ngr1*<sup>-/-</sup> mice display elevated frequency of mEPSCs with eye opening, this increase is only sustained in *ngr1*<sup>-/-</sup> mice.

(C) Cumulative distributions of mEPSC amplitudes for WT and *ngr1*<sup>-/-</sup> mice during LTMD and LTMD followed by 1 day and 4 weeks of binocular vision. *ngr1*<sup>-/-</sup> exhibits larger synaptic events at 1 day that are also evident at 4 weeks.

Error bars represent  $\pm$  SEM. See also Figure S3.

through the previously deprived eye immediately thereafter (Figure 5A). Mice with lower visual acuity fail the task at lower spatial frequencies in this behavioral assessment of visually guided performance (Figure 5B). WT and *ngr1*<sup>(f/f)</sup> mice exhibit a persistent deficit in visual acuity following LTMD (Figure 5C) [9, 10], whereas *ngr1*<sup>(-/-)</sup> mice recover normal visual acuity on this task with extended binocular vision [10].

First, we examined mice lacking *ngr1* in cortical excitatory neurons. The median threshold for visual acuity was lower in *ngr1*<sup>(f/f);CK-Cre</sup> mice following LTMD than in non-deprived controls (Figure 5C;  $p = 0.0002$ ; KW test). Surprisingly, although deleting *ngr1* selectively in cortex permitted the restoration of normal eye dominance (Figure 4), it did not promote recovery of acuity. In contrast, when *ngr1* was deleted from thalamus, visual acuity for these mice was indistinguishable from non-deprived controls (Figure 5E;  $p > 0.9$  flx versus flx;Scnn1a-Cre and flx versus flx;Olig3-Cre). Thus, abolishing NgR1 expression in thalamus permits recovery of visual acuity by the previously deprived eye in murine amblyopia despite abnormal eye dominance.

NgR1 is also expressed in the retina [29], and we considered the alternative hypothesis that NgR1 limits the recovery of acuity by preventing experience-dependent remodeling in this earliest structure in the visual pathway. To examine the potential contribution of plasticity limited by *ngr1* in the retina to the recovery of visual acuity, we examined the recombination of *ngr1*<sup>(f/f)</sup> sections of retina from each of the strains tested for recovery of eye dominance and acuity (Figure S6; related to Figure 5). We stained retinas of *ngr1*<sup>(f/f)</sup>, *ngr1*<sup>(f/f);CK-Cre</sup>, *ngr1*<sup>(f/f);Scnn1a-Cre</sup>, and *ngr1*<sup>(f/f);Olig3-Cre</sup> mice for GFP, a marker of Cre-mediated deletion of *ngr1* (Figure S4). The *ngr1*<sup>(f/f)</sup> allele was recombined in a subset of cells in the retina of *ngr1*<sup>(f/f);Scnn1a-Cre</sup> and *ngr1*<sup>(f/f);CK-Cre</sup> mice, but not *ngr1*<sup>(f/f)</sup> or *ngr1*<sup>(f/f);Olig3-Cre</sup> mice. The absence of recombination paired with the recovery of visual acuity in *ngr1*<sup>(f/f);Olig3-Cre</sup> mice does not support a role for NgR1 in retina to promote the recovery of acuity.

#### Deleting *ngr1* after the Onset of Amblyopia Promotes Recovery of Visual Acuity

To assess the potential therapeutic relevance of neutralizing NgR1 for treating amblyopia in adults, we used a pharmacoge-

netic approach to delete *ngr1* after the closure of the critical period. We employed the *ngr1*<sup>(f/f)</sup> allele together with a fusion protein linking Cre-recombinase with a mutated version of the estrogen receptor (*ER-Cre*) [30] (Figure 6A). Tamoxifen injection into *ngr1*<sup>(f/f);ER-Cre</sup> mice abolishes NgR1 expression within 7 days (Figure 6B) [17]. Mice received tamoxifen (1 mg/10 g intraperitoneally [i.p.] for 3 days) immediately before eye re-opening at P42 after the closure of the critical period ( $\sim$ P32). Thereafter, we measured visual acuity with the VWT after 6 weeks of binocular vision. When NgR1 expression was abolished in these young adult mice ( $\sim$ P50), visual acuity after 6 weeks of binocular vision was near normal and significantly greater than *ngr1*<sup>(f/f)</sup> controls, which were also treated with tamoxifen ( $p = 0.0003$ ; MW test; Figure 6C). Thus, abolishing NgR1 expression after the critical period improves acuity in this murine model of amblyopia.

## DISCUSSION

Amblyopia comprises several deficits in spatial vision, but the relationships between these different facets of vision remain poorly understood. A predominant model for the pathophysiology of amblyopia holds that abnormal vision engages OD plasticity during the critical period to exaggerate eye dominance, which in turn impairs visual performance through the affected eye, and these maladaptive changes to visual circuitry are consolidated with the close of the critical period. Consequently, re-opening the critical period for eye dominance has been considered central to the effective treatment of amblyopia, and approaches to enhance OD plasticity have been pursued for nearly 30 years [31]. Yet the fundamental relationship between eye dominance and acuity has not been resolved. The results presented here reveal that the neural circuit mechanisms underlying recovery of these two components of visual system function are independent.

In animal models for amblyopia, including rodents, MD shifts eye dominance away from the affected eye and reduces acuity [3, 9, 32, 33]. Several manipulations that promote OD plasticity after the critical period also promote recovery of visual acuity following LTMD [34]. Environmental manipulations, including environmental enrichment and dark exposure, enhance OD plasticity and increase visual acuity following LTMD [29, 35, 36].

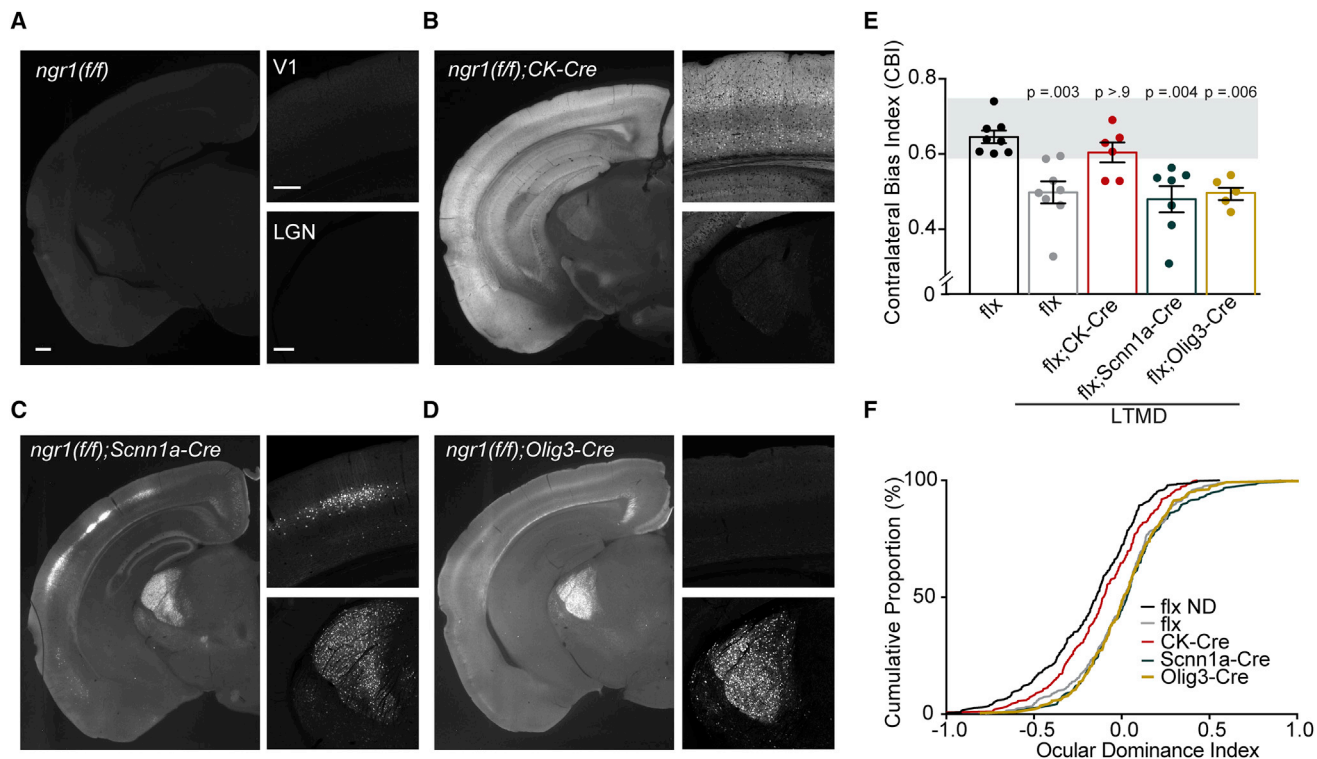


**Figure 4. Recovery of Eye Dominance following LTMD Is Restricted in Neocortex by *ngr1***

(A) Immunostaining for GFP in a coronal section from a *ngr1(ff)* mouse. Positive staining for GFP indicates recombination of the *ngr1(ff)* gene. The top right panel is an enlargement of V1, and the bottom right panel is an enlargement of thalamus from the same section as the wide field image on the left. The scale bars represent 225  $\mu$ m.

(B–D) Immunostaining for GFP as in (A) for (B) *ngr1(ff);CK-Cre*, (C) *ngr1(ff);Scnn1a-Cre*, and (D) *ngr1(ff);Olig3-Cre* mice.

(E) CBI scores for *ngr1(ff)* (flx) non-deprived mice (ND) (n = 8), as well as flx (n = 8), flx;CK-Cre (n = 6), flx;Scnn1a-Cre (n = 7), and flx;Olig3-Cre (n = 5) following LTMD and 6 weeks of binocular vision. Groups receiving LTMD are underlined. The gray box indicates the typical range of CBI values for non-deprived mice. Bars represent the average CBI score for each group with error bars for SEM. p values for Kruskal-Wallis (KW) multiple comparison tests with Dunn's correction to flx ND are presented above each column.

(F) Cumulative histograms of ocular dominance index (ODI) scores for flx ND (336 units), flx LTMD (326 units), flx;CK-Cre LTMD (240 units), flx;Scnn1a-Cre LTMD (296 units), and flx;Olig3-Cre LTMD (229 units).

Error bars represent  $\pm$  SEM. See also [Figures S4](#) and [S5](#).

Pharmacologic interventions also link OD plasticity and visual acuity. Rats treated with fluoxetine, a serotonin-specific reuptake inhibitor, or physostigmine, a cholinesterase inhibitor, display OD plasticity as adults and greater visual acuity following LTMD [37, 38]. In addition, two genes that are also required to close the critical period, *lynx1* and *pirb*, have also been implicated as factors that limit acuity [38, 39]. These latter studies employ visually evoked potentials (VEPs) to estimate acuity, whereas we have demonstrated that *ngr1* limits improvement of behavioral acuity. Where within the circuitry of the visual system any of these approaches may operate to promote the plasticity requisite for restoration of eye dominance and acuity remains unknown.

An early and essential component of OD plasticity during the critical period is a decrease in excitatory synaptic drive onto PV interneurons with MD [20]. NgR1 confines this disinhibition to the critical period [18]. Here, we demonstrate that *ngr1* mutant mice recover normal eye dominance with restoration of binocular vision following LTMD. Opening the closed eye following LTMD returns the major source of sensory input to visual cor-

tex. One day of normal vision increased excitatory synaptic drive onto PV interneurons in visual cortex in both WT and *ngr1* mutants, but the relative magnitude was substantially greater in *ngr1(-/-)* mice. Restoring binocular vision also resulted in a sustained elevation of mEPSC frequency and magnitude by L4 pyramidal neurons in *ngr1(-/-)* mice. These synaptic changes preceded eventual improvements in eye dominance and acuity by several weeks. As adult *ngr1(-/-)* mice recover both eye dominance and acuity, this provides a framework for identifying the neural circuits that limit recovery of these facets of visual function in the murine model of amblyopia.

Here, we employed a genetic dissection strategy to determine where *ngr1* expression is required to limit recovery of eye dominance and improvement of acuity following restoration of binocular vision. Genetic and pharmacologic studies identify visual cortex as the locus of OD plasticity [21, 40, 41], but recent reports have also implicated thalamus [23, 24]. We determined that abolishing *ngr1* expression in excitatory cortical neurons with *CK-Cre* permitted the recovery of eye dominance. Yet the

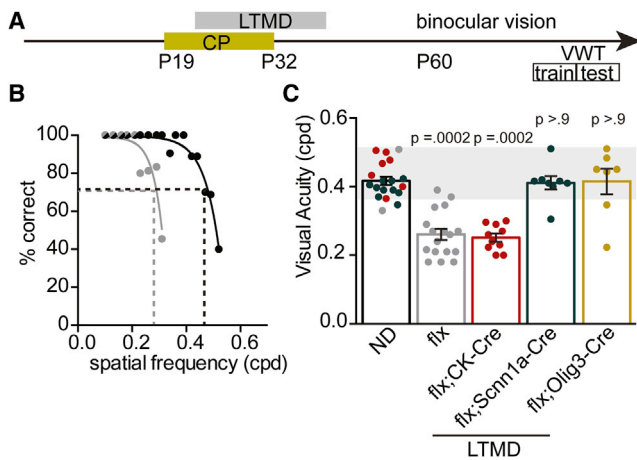


**Figure 5. Thalamus Restricts Recovery of Visual Acuity following LTMD**

(A) Schematic of the timeline for LTMD and the period of binocular vision prior to the visual water task (VWT) to assess visual acuity in adult (P90) mice. The VWT proceeds in two phases: training and testing.  
 (B) Performance of a representative *ngn1(f/f)* mouse that is non-deprived (black) or has received LTMD (gray).  
 (C) Acuity of ND *ngn1(f/f)* mice ( $n = 19$ ) measured through one eye, and acuity following LTMD and 6 weeks of binocular vision for *ngn1(f/f)* (*flx*) ( $n = 17$ ), *ngn1(f/f); CK-Cre* (*flx;CK-Cre*) ( $n = 10$ ), *ngn1(f/f); Scnn1a-Cre* (*flx;Scnn1a-Cre*) ( $n = 8$ ), and *ngn1(f/f); Olig3-Cre* (*flx;Olig3-Cre*) mice ( $n = 7$ ) measured through the previously deprived eye. Groups having received LTMD are underlined. Error bars represent  $\pm$  SEM. See also Figure S6.

restoration of normal eye dominance in *ngn1 flx/flx;CK-Cre* mice was insufficient to improve acuity. By comparison, deleting *ngn1* selectively in L4 excitatory neurons and thalamus with *Scnn1a-Cre* or thalamus alone with *Olig3-Cre* did not affect eye dominance, which remained similar to *ngn1 flx* mice lacking Cre expression and WT mice.

NgR1 does not appear to function by limiting cell-intrinsic OD plasticity. Deleting *ngn1* in L4 with *Scnn1a-Cre* does not yield cell-intrinsic recovery of eye dominance confined to L4. Reciprocally, abolishing *ngn1* in PV interneurons promotes OD plasticity by putative excitatory neurons across all layers of V1 following 4 days of MD [10]. We propose that *ngn1* gates OD plasticity for the cortical circuit as a whole rather than operating independently within each layer.

Unexpectedly, acuity recovered to normal levels in both *ngn1 flx/flx; Scnn1a-Cre* and *ngn1 flx/flx; Olig3-Cre* mice. These findings with two distinct Cre driver lines that direct expression in thalamus implicate plasticity within neurons of this subcortical structure as sufficient to improve acuity following LTMD. The independent recovery of eye dominance and acuity challenge the notion that mechanisms for OD plasticity contribute to the alterations in circuitry required to improve acuity in amblyopia.

The circuit alterations induced by visual deprivation that impair acuity have not been elucidated. We propose that alterations to thalamocortical circuits rather than abnormal eye dominance are a principal constraint on recovery of acuity in the mouse visual system following early abnormal vision. Low acuity may be a consequence of an overall shift in the tuning of neurons in thalamus and/or V1 to lower spatial frequencies or lower spatial frequency cutoffs for the population of neurons tuned to the highest

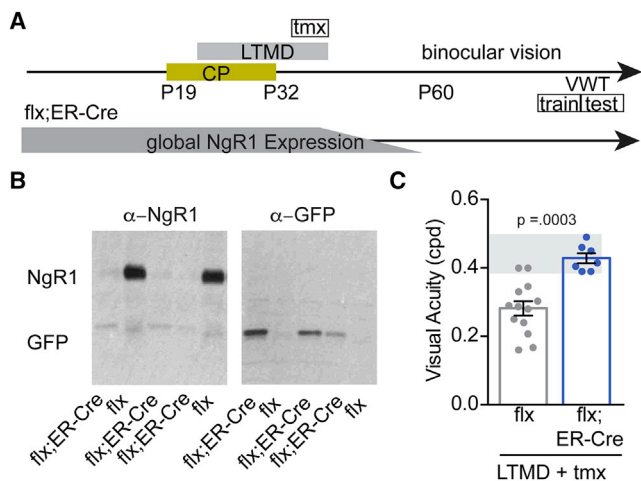


**Figure 6. Visual Acuity Is Restored following LTMD with Deletion of *ngn1* after the Critical Period**

(A) Schematic of the timeline for tamoxifen (tmx) administration and LTMD prior to the period of binocular vision that precedes the VWT to assess visual acuity in adult (P90) mice. The VWT proceeds in two phases: training and testing. Following administration of tamoxifen (tmx), the global expression of NgR1 is nearly completely absent after 7 days.  
 (B) Representative immunoblots confirm the recombination of *ngn1* in *ngn1(f/f); ER-Cre* (*flx;ER-Cre*) mice following testing on the VWT.  
 (C) Acuity following LTMD and 6 weeks of binocular vision for *ngn1(f/f)* (*flx*) ( $n = 13$ ) and *ngn1(f/f);ER-Cre* (*flx;ER-Cre*) ( $n = 7$ ) mice measured through the previously deprived eye. Groups having received LTMD and treatment with tamoxifen are underlined. Error bars represent  $\pm$  SEM.

spatial frequencies. We anticipate these tuning properties either arise in thalamus and/or visual cortex independent of eye dominance. However, one study has reported a slight increase in average spatial tuning for neurons with greater contralateral bias [42].

Consequently, characterizing how NgR1 may function to limit recovery of acuity within thalamic circuits will require further study. Several mechanisms for the loss and recovery of acuity have been proposed, including contrast sensitivity and inhibitory tone. When TrkB signaling is inhibited in adult mice, acuity estimated by intrinsic signal imaging of V1 decreases whereas OD plasticity and receptive field size are unaffected [43]. This lower acuity was correlated with a reduction in perceived contrast. However, perceived contrast sensitivity is cortex dependent [44], whereas *ngn1* operates in thalamic neurons to limit recovery of acuity. Pharmacologic and environmental manipulations proposed to decrease inhibitory tone are also associated with improvements in visual acuity following LTMD [45]. *NgR1(-/-)* mice exhibit a slight decrease in cortical inhibition and improved acuity following LTMD. However, this reduction in cortical inhibition is also present when *ngn1* is deleted from PV interneurons (*ngn1(f/f);PV-Cre*), yet there is no associated recovery of visual acuity despite sustained OD plasticity with brief MD [10].

A third possibility is neutralizing extracellular factors that restrict anatomical plasticity could contribute to improving acuity following LTMD. The digestion of chondroitin sulfate proteoglycans (CSPGs) in visual cortex by chondroitinase ABC (chABC) promotes OD plasticity and the recovery of acuity following

LTMD in rats [41, 46]. NgR1 is a receptor for CSPGs as well as inhibitors of neurite outgrowth associated with myelin membranes [14, 15]. CSPGs are enriched around PV interneurons in visual cortex, and these structures elaborate with the closure of the critical period and maturation of visual acuity [47]. One possible mechanism is that NgR1 operates presynaptically on thalamocortical axons to impede recovery of acuity following LTMD by binding CSPGs tethered to perineuronal nets and limiting the experience-dependent reorganization of synaptic connections by thalamic relay neurons onto PV interneurons and nearby pyramidal neurons.

Spine density is decreased in V1 following LTMD in the hemisphere contralateral to the deprivation and restored by several approaches that both promote OD plasticity and improve acuity, including injection of chABC (reviewed by [45]). NgR1 has been proposed as a regulator of the set point for spine dynamics. Suppressing NgR1 expression in primary hippocampal neurons by RNAi increases the density of excitatory synapses *in vitro* [12], and *ngr1* mutant mice have been reported to display dramatically increased basal turnover of dendritic spines *in vivo* [48]. Yet, spine density is normal in *ngr1*( $-/-$ ) mice, and we are unable to reproduce the reported elevated spine dynamics *in vivo*, despite performing similar, if not identical, experiments [19, 49].

The recovery of acuity in mice lacking *ngr1* is markedly slower than that observed for several manipulations that also improve acuity. Chondroitinase ABC, fluoxetine, and a soluble competitive inhibitor of PirB are all reported to restore acuity following LTMD to normal levels within 7 days of administration [37, 39, 46]. In contrast, acuity in *ngr1*( $-/-$ ) mice 7 days after eye opening remains low and similar to WT mice. More than a month of binocular vision is required to improve acuity in *ngr1* mutant mice, a duration similar to the normal maturation of acuity measured with the visual water task [10]. Perhaps this more gradual recovery of acuity operates through mechanisms similar to this developmental process.

What then are the potential implications of these findings for the treatment of amblyopia? Mice possess a relatively small binocular zone and poor acuity [3, 28]. The significant redistribution of thalamocortical arbors with extended visual deprivation observed in predatory mammals is not evident in rodents as they lack OD columns [8, 50]. Differences in the branching of individual thalamocortical axons subserving the deprived and non-deprived eye have been reported in mice following LTMD, but these are subtle by comparison [8]. In addition, the magnitude of the shift in eye dominance and decrement in acuity is also less than that observed in cats and primates following early visual deprivation [16]. However, mice and cats exhibit comparable eye dominance with the return of binocular vision. In mice, the representation of the deprived eye in V1 is similar to the fellow eye with a month of binocular vision after LTMD. In kittens, a substantial fraction of cortical neurons also strongly respond to the deprived eye with a month of binocular vision following 7–10 days of MD during the critical period despite sustained low acuity [51, 52]. Thus, whereas the mouse may not recapitulate aspects of severe amblyopia, in which the cortical representation of the affected eye is quite low or non-detectable, the mouse shares characteristics with the cat for studying more moderate deficits in spatial vision resulting from visual deprivation.

The genetic resources for the mouse also provide opportunities for insight not possible in other species. In particular, the role of the thalamic circuitry in amblyopia has proven difficult to characterize. Several studies have measured decreased cellular acuity in LGN of amblyopic animals (e.g., [53]), whereas others have made similar measurements but did not observe any cellular deficits (e.g., [54]). Here, we employed conditional genetics only available in the mouse to demonstrate that plasticity within thalamic circuitry is sufficient for recovery of normal acuity. Moreover, many fundamental aspects of circuitry in the visual system are conserved between rodents and other mammals, including linear versus nonlinear spatial summation; contrast-invariant tuning; selectivity for stimulus parameters, such as orientation and spatial frequency; and the sensitivity of eye dominance and acuity to visual deprivation during a defined developmental critical period [55]. Thus, we propose that, whereas the more complex circuitry of the visual system in humans may present additional challenges to recovery from amblyopia, our findings here that the neural plasticity for the recovery of eye dominance and acuity are independent inform understanding of the clinical disorder.

## STAR★METHODS

Detailed methods are provided in the online version of this paper and include the following:

- KEY RESOURCES TABLE
- CONTACT FOR REAGENT AND RESOURCE SHARING
- EXPERIMENTAL MODEL AND SUBJECT DETAILS
  - Mice
- METHOD DETAILS
  - Monocular Deprivation (MD)
  - Electrophysiological Recordings in Visual Cortex
  - Immunohistochemistry
  - Patch clamp recording and LSPS
  - Visual Water Task
  - Tamoxifen Treatment
  - Immunoblotting
- QUANTIFICATION AND STATISTICAL ANALYSIS
- DATA AND SOFTWARE AVAILABILITY

## SUPPLEMENTAL INFORMATION

Supplemental Information includes six figures and can be found with this article online at <https://doi.org/10.1016/j.cub.2018.04.055>.

## ACKNOWLEDGMENTS

This research is supported by the National Eye Institute (R01EY021580 and R01EY027407), a Research Development Career Award from Children's Hospital Los Angeles, and the Disney Award for Amblyopia Research from Research to Prevent Blindness. C.E.S. is the recipient of a predoctoral fellowship from the Saban Research Institute. A.W.M. is the recipient of a Career Award in the Biomedical Sciences (CABS) from the Burroughs Wellcome Fund.

## AUTHOR CONTRIBUTIONS

C.-E.S., S.Q., and A.W.M. designed the study. C.-E.S., X.M., H.M.D., J.W., A.M.S., M.G.F., and S.Q. performed the experiments. C.-E.S., S.Q., and A.W.M. wrote the manuscript.

## DECLARATION OF INTERESTS

The authors declare no competing interests.

Received: February 5, 2018

Revised: March 20, 2018

Accepted: April 17, 2018

Published: June 7, 2018

## REFERENCES

1. Webber, A.L., and Wood, J. (2005). Amblyopia: prevalence, natural history, functional effects and treatment. *Clin. Exp. Optom.* **88**, 365–375.
2. Sengpiel, F. (2014). Plasticity of the visual cortex and treatment of amblyopia. *Curr. Biol.* **24**, R936–R940.
3. Gordon, J.A., and Stryker, M.P. (1996). Experience-dependent plasticity of binocular responses in the primary visual cortex of the mouse. *J. Neurosci.* **16**, 3274–3286.
4. Kratz, K.E., Mangel, S.C., Lehmkuhle, S., and Sherman, M. (1979). Retinal X- and Y-cells in monocularly lid-sutured cats: normality of spatial and temporal properties. *Brain Res.* **172**, 545–551.
5. Kiorpes, L. (2006). Visual processing in amblyopia: animal studies. *Strabismus* **14**, 3–10.
6. Dräger, U.C. (1978). Observations on monocular deprivation in mice. *J. Neurophysiol.* **41**, 28–42.
7. Fischer, Q.S., Aleem, S., Zhou, H., and Pham, T.A. (2007). Adult visual experience promotes recovery of primary visual cortex from long-term monocular deprivation. *Learn. Mem.* **14**, 573–580.
8. Antonini, A., Fagiolini, M., and Stryker, M.P. (1999). Anatomical correlates of functional plasticity in mouse visual cortex. *J. Neurosci.* **19**, 4388–4406.
9. Prusky, G.T., and Douglas, R.M. (2003). Developmental plasticity of mouse visual acuity. *Eur. J. Neurosci.* **17**, 167–173.
10. Stephany, C.-É., Chan, L.L.H., Parivash, S.N., Dorton, H.M., Piechowicz, M., Qiu, S., and McGee, A.W. (2014). Plasticity of binocularity and visual acuity are differentially limited by nogo receptor. *J. Neurosci.* **34**, 11631–11640.
11. Wang, X., Chun, S.-J., Treloar, H., Vartanian, T., Greer, C.A., and Strittmatter, S.M. (2002). Localization of Nogo-A and Nogo-66 receptor proteins at sites of axon-myelin and synaptic contact. *J. Neurosci.* **22**, 5505–5515.
12. Wills, Z.P., Mandel-Brehm, C., Mardinly, A.R., McCord, A.E., Giger, R.J., and Greenberg, M.E. (2012). The nogo receptor family restricts synapse number in the developing hippocampus. *Neuron* **73**, 466–481.
13. Barrette, B., Vallières, N., Dubé, M., and Lacroix, S. (2007). Expression profile of receptors for myelin-associated inhibitors of axonal regeneration in the intact and injured mouse central nervous system. *Mol. Cell. Neurosci.* **34**, 519–538.
14. Dickendesher, T.L., Baldwin, K.T., Mironova, Y.A., Koriyama, Y., Raiker, S.J., Askew, K.L., Wood, A., Geoffroy, C.G., Zheng, B., Liepmann, C.D., et al. (2012). NgR1 and NgR3 are receptors for chondroitin sulfate proteoglycans. *Nat. Neurosci.* **15**, 703–712.
15. Baldwin, K.T., and Giger, R.J. (2015). Insights into the physiological role of CNS regeneration inhibitors. *Front. Mol. Neurosci.* **8**, 23.
16. Stephany, C.-É., Frantz, M.G., and McGee, A.W. (2016). Multiple roles for Nogo receptor 1 in visual system plasticity. *Neuroscientist* **22**, 653–666.
17. Wang, X., Duffy, P., McGee, A.W., Hasan, O., Gould, G., Tu, N., Harel, N.Y., Huang, Y., Carson, R.E., Weinzimmer, D., et al. (2011). Recovery from chronic spinal cord contusion after Nogo receptor intervention. *Ann. Neurol.* **70**, 805–821.
18. Stephany, C.-É., Ikrar, T., Nguyen, C., Xu, X., and McGee, A.W. (2016). Nogo receptor 1 confines a disinhibitory microcircuit to the critical period in visual cortex. *J. Neurosci.* **36**, 11006–11012.
19. Frantz, M.G., Kast, R.J., Dorton, H.M., Chapman, K.S., and McGee, A.W. (2016). Nogo receptor 1 limits ocular dominance plasticity but not turnover of axonal boutons in a model of amblyopia. *Cereb. Cortex* **26**, 1975–1985.
20. Kuhlman, S.J., Olivas, N.D., Tring, E., Ikrar, T., Xu, X., and Trachtenberg, J.T. (2013). A disinhibitory microcircuit initiates critical-period plasticity in the visual cortex. *Nature* **501**, 543–546.
21. Taha, S., and Stryker, M.P. (2002). Rapid ocular dominance plasticity requires cortical but not geniculate protein synthesis. *Neuron* **34**, 425–436.
22. Howarth, M., Walmsley, L., and Brown, T.M. (2014). Binocular integration in the mouse lateral geniculate nuclei. *Curr. Biol.* **24**, 1241–1247.
23. Sommeijer, J.-P., Ahmadiou, M., Saiepour, M.H., Seignette, K., Min, R., Heimel, J.A., and Levelt, C.N. (2017). Thalamic inhibition regulates critical-period plasticity in visual cortex and thalamus. *Nat. Neurosci.* **20**, 1715–1721.
24. Jaepel, J., Hübener, M., Bonhoeffer, T., and Rose, T. (2017). Lateral geniculate neurons projecting to primary visual cortex show ocular dominance plasticity in adult mice. *Nat. Neurosci.* **20**, 1708–1714.
25. Tsien, J.Z., Chen, D.F., Gerber, D., Tom, C., Mercer, E.H., Anderson, D.J., Mayford, M., Kandel, E.R., and Tonegawa, S. (1996). Subregion- and cell type-restricted gene knockout in mouse brain. *Cell* **87**, 1317–1326.
26. Madisen, L., Zwingman, T.A., Sunkin, S.M., Oh, S.W., Zariwala, H.A., Gu, H., Ng, L.L., Palmiter, R.D., Hawrylycz, M.J., Jones, A.R., et al. (2010). A robust and high-throughput Cre reporting and characterization system for the whole mouse brain. *Nat. Neurosci.* **13**, 133–140.
27. Vue, T.Y., Lee, M., Tan, Y.E., Werkhoven, Z., Wang, L., and Nakagawa, Y. (2013). Thalamic control of neocortical area formation in mice. *J. Neurosci.* **33**, 8442–8453.
28. Prusky, G.T., West, P.W., and Douglas, R.M. (2000). Behavioral assessment of visual acuity in mice and rats. *Vision Res.* **40**, 2201–2209.
29. He, H.Y., Hodos, W., and Quinlan, E.M. (2006). Visual deprivation reactivates rapid ocular dominance plasticity in adult visual cortex. *J. Neurosci.* **26**, 2951–2955.
30. Hayashi, S., and McMahon, A.P. (2002). Efficient recombination in diverse tissues by a tamoxifen-inducible form of Cre: a tool for temporally regulated gene activation/inactivation in the mouse. *Dev. Biol.* **244**, 305–318.
31. Müller, C.M., and Best, J. (1989). Ocular dominance plasticity in adult cat visual cortex after transplantation of cultured astrocytes. *Nature* **342**, 427–430.
32. Wiesel, T.N., and Hubel, D.H. (1965). Extent of recovery from the effects of visual deprivation in kittens. *J. Neurophysiol.* **28**, 1060–1072.
33. Giffin, F., and Mitchell, D.E. (1978). The rate of recovery of vision after early monocular deprivation in kittens. *J. Physiol.* **274**, 511–537.
34. Levelt, C.N., and Hübener, M. (2012). Critical-period plasticity in the visual cortex. *Annu. Rev. Neurosci.* **35**, 309–330.
35. He, H.-Y., Ray, B., Dennis, K., and Quinlan, E.M. (2007). Experience-dependent recovery of vision following chronic deprivation amblyopia. *Nat. Neurosci.* **10**, 1134–1136.
36. Sale, A., Maya Vetencourt, J.F., Medini, P., Cenni, M.C., Baroncelli, L., De Pasquale, R., and Maffei, L. (2007). Environmental enrichment in adulthood promotes amblyopia recovery through a reduction of intracortical inhibition. *Nat. Neurosci.* **10**, 679–681.
37. Maya Vetencourt, J.F., Sale, A., Viegi, A., Baroncelli, L., De Pasquale, R., O’Leary, O.F., Castrén, E., and Maffei, L. (2008). The antidepressant fluoxetine restores plasticity in the adult visual cortex. *Science* **320**, 385–388.
38. Morishita, H., Miwa, J.M., Heintz, N., and Hensch, T.K. (2010). Lynx1, a cholinergic brake, limits plasticity in adult visual cortex. *Science* **330**, 1238–1240.
39. Bochner, D.N., Sapp, R.W., Adelson, J.D., Zhang, S., Lee, H., Djurisic, M., Syken, J., Dan, Y., and Shatz, C.J. (2014). Blocking PirB up-regulates spines and functional synapses to unlock visual cortical plasticity and facilitate recovery from amblyopia. *Sci. Transl. Med.* **6**, 258ra140.

40. Taha, S., Hanover, J.L., Silva, A.J., and Stryker, M.P. (2002). Autophosphorylation of alphaCaMKII is required for ocular dominance plasticity. *Neuron* 36, 483–491.
41. Pizzorusso, T., Medini, P., Berardi, N., Chierzi, S., Fawcett, J.W., and Maffei, L. (2002). Reactivation of ocular dominance plasticity in the adult visual cortex. *Science* 298, 1248–1251.
42. Salinas, K.J., Figueroa Velez, D.X., Zeitoun, J.H., Kim, H., and Gandhi, S.P. (2017). Contralateral bias of high spatial frequency tuning and cardinal direction selectivity in mouse visual cortex. *J. Neurosci.* 37, 10125–10138.
43. Heimel, J.A., Saiepour, M.H., Chakravarthy, S., Hermans, J.M., and Levitt, C.N. (2010). Contrast gain control and cortical TrkB signaling shape visual acuity. *Nat. Neurosci.* 13, 642–648.
44. Glickfeld, L.L., Histed, M.H., and Maunsell, J.H.R. (2013). Mouse primary visual cortex is used to detect both orientation and contrast changes. *J. Neurosci.* 33, 19416–19422.
45. Morishita, H., and Hensch, T.K. (2008). Critical period revisited: impact on vision. *Curr. Opin. Neurobiol.* 18, 101–107.
46. Pizzorusso, T., Medini, P., Landi, S., Baldini, S., Berardi, N., and Maffei, L. (2006). Structural and functional recovery from early monocular deprivation in adult rats. *Proc. Natl. Acad. Sci. USA* 103, 8517–8522.
47. Huang, Z.J., Kirkwood, A., Pizzorusso, T., Porciatti, V., Morales, B., Bear, M.F., Maffei, L., and Tonegawa, S. (1999). BDNF regulates the maturation of inhibition and the critical period of plasticity in mouse visual cortex. *Cell* 98, 739–755.
48. Akbik, F.V., Bhagat, S.M., Patel, P.R., Cafferty, W.B.J., and Strittmatter, S.M. (2013). Anatomical plasticity of adult brain is titrated by Nogo receptor 1. *Neuron* 77, 859–866.
49. Park, J.I., Frantz, M.G., Kast, R.J., Chapman, K.S., Dorton, H.M., Stephany, C.-É., Arnett, M.T., Herman, D.H., and McGee, A.W. (2014). Nogo receptor 1 limits tactile task performance independent of basal anatomical plasticity. *PLoS ONE* 9, e112678.
50. LeVay, S., Wiesel, T.N., and Hubel, D.H. (1980). The development of ocular dominance columns in normal and visually deprived monkeys. *J. Comp. Neurol.* 191, 1–51.
51. Olson, C.R., and Freeman, R.D. (1978). Monocular deprivation and recovery during sensitive period in kittens. *J. Neurophysiol.* 41, 65–74.
52. Duffy, K.R., and Mitchell, D.E. (2013). Darkness alters maturation of visual cortex and promotes fast recovery from monocular deprivation. *Curr. Biol.* 23, 382–386.
53. Maffei, L., and Fiorentini, A. (1976). Monocular deprivation in kittens impairs the spatial resolution of geniculate neurones. *Nature* 264, 754–755.
54. Derrington, A.M., and Hawken, M.J. (1981). Spatial and temporal properties of cat geniculate neurones after prolonged deprivation. *J. Physiol.* 314, 107–120.
55. Huberman, A.D., and Niell, C.M. (2011). What can mice tell us about how vision works? *Trends Neurosci.* 34, 464–473.
56. Kim, J.-E., Liu, B.P., Park, J.H., and Strittmatter, S.M. (2004). Nogo-66 receptor prevents raphespinal and rubrospinal axon regeneration and limits functional recovery from spinal cord injury. *Neuron* 44, 439–451.
57. Qiu, S., Anderson, C.T., Levitt, P., and Shepherd, G.M.G. (2011). Circuit-specific intracortical hyperconnectivity in mice with deletion of the autism-associated Met receptor tyrosine kinase. *J. Neurosci.* 31, 5855–5864.
58. McGee, A.W., Yang, Y., Fischer, Q.S., Daw, N.W., and Strittmatter, S.M. (2005). Experience-driven plasticity of visual cortex limited by myelin and Nogo receptor. *Science* 309, 2222–2226.
59. Piscopo, D.M., El-Danaf, R.N., Huberman, A.D., and Niell, C.M. (2013). Diverse visual features encoded in mouse lateral geniculate nucleus. *J. Neurosci.* 33, 4642–4656.
60. Wiesel, T.N., and Hubel, D.H. (1963). Single-cell responses in striate cortex of kittens deprived of vision in one eye. *J. Neurophysiol.* 26, 1003–1017.
61. Hirano, A.A., Brandstätter, J.H., and Brecha, N.C. (2005). Cellular distribution and subcellular localization of molecular components of vesicular transmitter release in horizontal cells of rabbit retina. *J. Comp. Neurol.* 488, 70–81.
62. Xu, X., and Callaway, E.M. (2009). Laminar specificity of functional input to distinct types of inhibitory cortical neurons. *J. Neurosci.* 29, 70–85.
63. Shepherd, G.M.G., and Svoboda, K. (2005). Laminar and columnar organization of ascending excitatory projections to layer 2/3 pyramidal neurons in rat barrel cortex. *J. Neurosci.* 25, 5670–5679.
64. Weiler, N., Wood, L., Yu, J., Solla, S.A., and Shepherd, G.M.G. (2008). Top-down laminar organization of the excitatory network in motor cortex. *Nat. Neurosci.* 11, 360–366.

## STAR★METHODS

### KEY RESOURCES TABLE

REAGENT or RESOURCE	SOURCE	IDENTIFIER
<b>Antibodies</b>		
Rabbit polyclonal anti-GFP	Novus	Cat#NB600-308; RRID: AB_10003058
Rabbit polyclonal anti-GFP	Molecular Probes	Cat#: A-21311; RRID: AB_221477
Rabbit polyclonal anti-GFP	GeneTex	Cat#GTX26556 RRID: AB_371421
Goat polyclonal anti-Ngr1	R&D Systems	Cat#AF-1440; RRID: AB_218373
<b>Experimental Models: Organisms/Strains</b>		
Mouse: C57Bl6J - rtn4r KO	[56]	N/A
Mouse: C57Bl6J - rtn4r flx	[17]	N/A
Mouse: C57Bl6J	The Jackson Laboratory	JAX: 00664
Mouse: B6.129P2- <i>Pvalb</i> <sup>tm1(cre)Arbr/J</sup>	The Jackson Laboratory	JAX: 017320
Mouse: B6.Cg-Gt( <i>ROSA</i> )26Sor <sup>tm14(CAG-tdTomato)Hze/J</sup>	The Jackson Laboratory	JAX: 007914
Mouse: B6.Cg-Tg( <i>Camk2a-cre</i> )T29-1Stl/J	The Jackson Laboratory	JAX: 005359
Mouse: B6;C3-Tg( <i>Scnn1a-cre</i> )3Aibs/J	The Jackson Laboratory	JAX: 009613
Mouse: B6.Cg-Tg( <i>CAG-cre</i> /Esr1*)5Amc/J	The Jackson Laboratory	JAX: 004682
Mouse: <i>Olig3</i> <sup>tm1(cre)Ynka</sup>	[27]	N/A
<b>Oligonucleotides</b>		
Ngr1 WT F: cag tac ctg cga ctc aat gac	[56]	N/A
NgR1 WT R: ctt ccg gga aca acc tgg cct cc	[56]	N/A
Neo F: ta ttc ggc tat gac tgg gca	[56]	N/A
Neo R: gaa ctc gtc aag aag gcg ata	[56]	N/A
CRE F: ccg gtc gat gca acg agt gat gag gtt cgc	This paper	N/A
CRE R: ctc gac cag ttt agt tac ccc cag gct aag	This paper	N/A
NgR1 flx R: gcg gat ctt gaa gtt cac ctt	This paper	N/A
NgR1 flx/WT F: gag ctg aca tcc atg agc tca gcc	This paper	N/A
NgR1 WT R: ggg aga cag acc cat tcc tgg tcc ctc aca acc	This paper	N/A
NgR1 delta F: tgg tga cca att ggg cta gcc ctg tgg	This paper	N/A
<b>Software and Algorithms</b>		
Spike2 Software	CED	RRID: SCR_000903
MATLAB	Mathworks	RRID: SCR_001622
MATLAB visual stimulus scripts	[10]	N/A
MATLAB LSPS scripts	[57]	N/A

### CONTACT FOR REAGENT AND RESOURCE SHARING

Further information and requests for resources and reagents should be directed to and will be fulfilled by the lead contact, Aaron W. McGee ([aaron.mcgee@louisville.edu](mailto:aaron.mcgee@louisville.edu)). Requests for mouse strains developed by third parties will be directed to the appropriate contact.

### EXPERIMENTAL MODEL AND SUBJECT DETAILS

#### Mice

The constitutive *ngr1/rtn4r* (−/−) and conditional *ngr1/rtn4r* (*flx/flx*) mouse strains were a gift of Dr. Stephen Strittmatter, Yale University School of Medicine [17, 56]. The constitutive mutant mice had been repeatedly backcrossed onto the C57Bl6J background to at least F8. WT (C57Bl6J; The Jackson Laboratory, strain 00664) and *ngr1* (−/−) were crossed onto the background *PV-Cre; Ai14(RCL-tdT)* for LSPS circuit mapping (strain numbers 017320 and 007914, respectively) [10].

The conditional strain to F6 before being rederived (strain number 00664). The *ngr1(f/f)* line was backcrossed against the C57Bl6J background to at least F8. Subsequently, the *ngr1(f/f)* line was backcrossed against C57Bl6J with either the *CK-Cre*, *Scnn1a-Cre*, *Olig3-Cre* or *ER-Cre* driver strains [25, 26, 30]. The *CK-Cre*, *Scnn1a-Cre*, and *ER-Cre* driver strains were imported from Jackson Labs (strain numbers 005359, 009613, 004682, respectively). The *Olig3-Cre* driver line was a generous gift of Dr. Yasushi Nakagawa (University of Minnesota) [27].

Experiments and procedures were performed on both adult male and female mice by an experimenter blind to genotype. Mice were group housed and maintained on a 12-hr light/dark cycle under standard housing conditions. For experimental and control groups including the *ngr1(f/f)* line, experiments were performed on littermates. Genotyping was performed using custom primer sets for polymerase chain reaction (PCR) amplification with REExtract-N-Amp PCR kit (XNAT, Sigma). Mice for the *ngr1(f/f) ± Cre* groups were generated by crossing *ngr1(f/f); Cre* dams with *ngr1(f/f)* males. All mice were genotyped for germline recombination of the *ngr1* allele. Mice with germline recombination were ejected from the study.

All procedures and care were performed in accordance with the guidelines of the Institutional Animal Care and Use Committees at Children's Hospital Los Angeles and the University of Louisville.

## METHOD DETAILS

### Monocular Deprivation (MD)

One eye was closed on postnatal day 24 (P24) using a single mattress suture tied with 6-0 polypropylene monofilament (Prolene 8709H; Ethicon) under brief isoflurane anesthesia (2%). The knot was sealed with cyanoacrylate glue. The suture was removed 3 weeks later at P45 with fine iridectomy scissors and the eyes were flushed with sterile saline. The eye was examined under a stereomicroscope and animals with scarring of the cornea were eliminated from the study. Following eye-opening, mice received a 6-week period of binocular vision prior to electrophysiological recording or the visual water task.

### Electrophysiological Recordings in Visual Cortex

Recording methods were adapted from previously published methods [10, 58]. In brief, mice were anesthetized with isoflurane (4% induction, 2% maintenance in O<sub>2</sub> during surgery) rather than barbiturates (Nembutal) as we have used in preceding studies [10, 58]. The mouse was placed in a stereotaxic frame and temperature was maintained at 37°C by a homeostatically-regulated heat pad (TCAT-2LV, Physitemp). Dexamethasone (4 mg/kg s.c.; American Reagent) was administered to reduce cerebral edema. The eyes were flushed with saline and the corneas were protected thereafter by covering the eyes throughout the surgical procedure and with frequent application of saline. A craniotomy was made over visual cortex in the left hemisphere and a metallic head bar was attached with cyanoacrylate glue over the right hemisphere to immobilize the animal during recording. Prior to transfer to the recording setup, a dose of chlorprothixene (0.5 mg/kg i.p.; C1761, Sigma) was administered to decrease the level of isoflurane required to maintain anesthesia to 0.6% [59].

Recordings were made with EpoxyLite-coated tungsten microelectrodes with tip resistances of 5–10 MΩ (FHC). The signal was amplified (model 3600; A-M Systems), low-pass filtered at 3000Hz, high-pass filtered at 300Hz, and digitized (micro1401; Cambridge Electronic Design). Single-unit activity was recorded from four to six locations separated by > 90 μm in depth for each electrode penetration. In each mouse, there were four to six penetrations separated by at least 200 μm across the binocular region of primary visual cortex, defined by a receptive field azimuth < 25°. Responses were driven by drifting sinusoidal gratings (0.1 cpd, 95% contrast), presented in six orientations separated by 30° (custom software, MATLAB) [10]. The gratings were presented for 2 s of each 4 s trial. The grating was presented in each orientation in a pseudorandom order at least four times, interleaved randomly by a blank, which preceded each orientation once. Action potentials (APs) were identified in recorded traces with Spike2 (Cambridge Electronic Design). Only waveforms extending beyond 4 standard deviations above the average noise were included in subsequent analysis. For each unit, the number of APs in response to the grating stimuli was summed and averaged over the number of presentations. If the average number of APs for the grating stimuli was not greater than 50% above the blank, the unit was discarded.

The ocular dominance index (ODI) was calculated for each unit by comparing the number of APs elicited in a given unit when showing the same visual stimulus to each eye independently. Units were assigned to one of seven OD categories (1-7) where units assigned to category 1 are largely dominated by input from the contralateral eye, and units assigned to category 7 are largely dominated by input from the ipsilateral eye [60]. To categorize each unit, the average number of APs elicited by the blank was subtracted from the average number of APs elicited by the gratings for the contralateral eye (CE) and the ipsilateral eye (IE). Next, the ocular dominance index (ODI), given by  $ODI = (IE - CE) / (IE + CE)$  was calculated for each unit and assigned to OD categories 1-7 as follows: -1 to -0.6 = 1, -0.6 to -0.4 = 2, -0.4 to -0.1 = 3, -0.1 to 0.1 = 4, 0.1 to 0.4 = 5, 0.4 to 0.6 = 6, 0.6 to 1 = 7. Finally, the sum of the number of cells in each category was used to calculate the CBI for each animal with the formula:  $CBI = [(n1 - n7) + (2/3)(n2 - n6) + (1/3)(n3 - n5) + N] / 2N$  where N is the total number of units and  $n_x$  is the number of units with OD scores equal to x [3].

### Immunohistochemistry

Mice were deeply anesthetized with Ketamine HCl (200mg/kg, Phoenix pharmaceuticals)/Xylazine (20mg/kg, Lloyd Laboratories) and the eyes were enucleated prior to transcardial perfusion with phosphate buffered saline (PBS; ChemCruz SC-362299) followed by a buffered 4% paraformaldehyde (PFA)/PBS (Acros Organics 416780030). Eyes were dissected in refrigerated HyClone Dulbecco's Modified Eagles Medium (GE Healthcare Life Sciences). The eyecups were then immersion-fixed in 4% PFA/PBS for

1 hr and cryoprotected overnight in 30% sucrose. The eyecups were then sectioned at 16–20  $\mu\text{m}$  with a cryostat (Leica Microsystems), mounted onto SuperFrost Plus slides (Fischer), and stored at  $-20^{\circ}\text{C}$ . Brains post-fixed overnight in 4% PFA/PBS. Free-floating 50  $\mu\text{m}$  sections were cut on a vibrating microtome (Leica VT 1000S) in cool PBS and preserved in PBS containing 0.05% sodium azide (Sigma-Aldrich S8032).

Coronal sections containing visual cortex and LGN were washed in PBS (3  $\times$  5 min) and incubated in blocking solution, 3% normal donkey serum (NDS; Jackson ImmunoResearch) in PBS containing 0.1% Triton X-100 (Sigma-Aldrich T9284) (PBS-T) for 1 h at room temperature. The primary antibody rabbit anti-GFP (Novus, NB600-308) was diluted in blocking solution to 1  $\mu\text{g}/\text{ml}$  and sections incubated in primary antibody overnight at  $4^{\circ}\text{C}$ . After repeated washing in PBS-T (3  $\times$  30 min), sections were incubated in Alexa 488-conjugated secondary antibody (Jackson Immuno Research, 1:200 in blocking solution) overnight at  $4^{\circ}\text{C}$ . The first among a final series of washes contained Hoechst (1:10000 in PBS-T, Santa Cruz Biotech)(1  $\times$  10min), followed by PBS-T (2  $\times$  30min) and PBS (1  $\times$  10min). Finally, sections were mounted onto SuperFrost Plus slides (Fisher) with SlowFade Gold anti-fade reagent (Life technologies). Images of the entire hemisphere containing V1 and LGN were captured using a Leica MZFLIII fluorescence stereoscope with a 1.0X PLAN-APO lens. High-magnification images of V1 and LGN from coronal sections stained with anti-GFP were captured with an LSM-710 confocal microscope with a 20X 0.4 NA objective (Zeiss). Hoechst staining was utilized to demarcate visual cortex and LGN. Several images were required to capture the entirety of V1 and LGN. Images were merged with Zeiss ZEN software.

Immunohistochemical labeling of retinal sections was performed as previously described [61]. Retinal sections were incubated in a solution of 10% NDS and 0.5% Triton X-100 in 0.1M PBS for 1 h at room temperature. The blocking solution was washed away and the sections were incubated for 12–16 h at  $4^{\circ}\text{C}$  in a humidified chamber in the dark in a primary antibody solution containing the primary anti-GFP antibody (2.5  $\mu\text{g}/\text{ml}$ ) (Molecular Probes, A-21311), 3%NDS, and 0.5% Triton X-100 in 0.1M PBS. The primary antibody was directly conjugated to Alexa 488. Then, retinal sections were washed in PBS, and incubated in a control Alexa 594-conjugated secondary antibody (2  $\mu\text{g}/\text{ml}$ ) (Jackson Immuno Research) for 1 h at room temperature in the dark. After a final wash, the sections were coverslipped with Fluoromount-G (Southern Biotech). Images of the retina were captured with an LSM-710 confocal microscope with a 20X 0.4 NA objective (Zeiss).

### Patch clamp recording and LSPS

Recording methods are previously published [10, 57]. Electrophysiological recording and LSPS mapping experiments were performed on P45–50 and P110–120 mice on the background PV-Cre; Ai14. Mice were decapitated under deep isoflurane anesthesia. The visual cortex at the level of V1 was sectioned into 350  $\mu\text{m}$  coronal slices using a vibratome (VT1200S; Leica Systems) in ice-cold artificial cerebrospinal fluid (ACSF, containing in mM: 126 NaCl, 26  $\text{NaHCO}_3$ , 2  $\text{CaCl}_2$ , 2  $\text{MgCl}_2$ , 2.5 KCl, 1.25  $\text{NaH}_2\text{PO}_4$ , and 10 glucose). The slices were then incubated for 30 min at  $32^{\circ}\text{C}$  in ACSF saturated with 95%  $\text{O}_2$  and 5%  $\text{CO}_2$ , and maintained at room temperature in ACSF for at least 30 min before being used for recording.

Visual cortex slices were transferred to a recording chamber mounted on a motorized stage (Sutter Instruments, Novato, CA), visualized with a microscope (BX51WI; Olympus, Tokyo, Japan) under infrared differential interference contrast (DIC) optics and an epifluorescent light source. The V1 binocular zone was identified based on the laminar and cytoarchitectonic features and the coordinates [62]. Patch clamp recording and LSPS mapping were performed as described previously [57]. Slices were first visualized with a 4X objective (NA 0.13, Olympus) to select the laminar location of neurons. Digital slice images were then acquired with a CCD camera (Retiga 2000DC, Qimaging, Surrey, BC, Canada), and used for registering photostimulation locations. Neurons were then patch clamped with a 60X water immersion objective (LUMPlanFI, NA 0.9, Olympus). PV interneurons (labeled by td-Tomato) in binocular zone were identified under DIC and epifluorescence for patch clamp whole-cell recording. Electrophysiological signals were amplified with a Multiclamp 700B amplifier (Molecular Devices, Sunnyvale, CA) and digitized at 10 kHz with BNC 6259 data acquisition boards (National Instruments, Austin, TX) that are controlled by Ephus software (<https://openwiki.janelia.org/>). The patch electrode was pulled from borosilicate glass (4–6 M $\Omega$  electrical resistance). Intrinsic neuronal properties were measured in current-clamp mode by injecting current steps (1 s duration,  $-100$  to  $+500$  pA in 50 pA increments), from which current injection – firing frequency was calculated. Series resistance ( $R_s$ ) was monitored throughout recordings in voltage clamp mode, only stable ( $< 15\%$  change) cells with  $R_s < 30$  M $\Omega$  throughout the recordings were included for analyses.

LSPS mapping on visual cortex slices was carried out at room temperature. The chamber was perfused with modified ACSF with higher concentrations of magnesium and calcium (in mM: 126 NaCl, 2.5 KCl, 26  $\text{NaHCO}_3$ , 4  $\text{CaCl}_2$ , 4  $\text{MgCl}_2$ , 1.25  $\text{NaH}_2\text{PO}_4$ , and 10 glucose) at 2–3 mL/min [57]. This modified ACSF also contains 5  $\mu\text{M}$  R-CPP (to block NMDA-receptor currents and plasticity) and 0.2 mM MNI-caged glutamate (both from Tocris-Cookson). The electrode internal solution contains (in mM) 130 K-gluconate, 4 KCl, 2 NaCl, 10 HEPES, 4 ATP-Mg, 0.3 GTP-Na and 14 phosphocreatine (pHc7.2, 295cmOsm). Neuronal cell bodies were at least 50  $\mu\text{m}$  below the surface of the slice to maximize preservation of local cortical connectivity. LSPS was performed through a 4  $\times$  objective lens (NA 0.13, Olympus). 20-mW, 1-ms UV laser (350nm, DPSS Lasers) pulses were scanned onto the sample after passing an electro-optical modulator (Conoptics, Danbury, CT) and a mechanical shutter (Uniblitz, Rochester, NY). Triggered acquisition of whole cell currents in patch-clamped neurons were recorded under voltage clamp. A stimulus grid (16  $\times$  16, 75  $\mu\text{m}$  spacing) was overlaid on the binocular V1 region, spanning from pia to white matter. For each L2/3 PV neuron, the stimulation grid was centered horizontally over the soma, and the top row was aligned with the pia. PV neurons were voltage clamped at  $-70\text{mV}$  during

the LSPS UV laser uncaging. In some experiments where excitation profiles were collected from L4 neurons [57, 63, 64], which provide major synaptic inputs to the L2/3 PV neurons, loose-seal recordings were made from these L4 pyramidal neurons. The spike-generating sites of neurons were mapped using an 8-by-8 stimulus grid with 50  $\mu\text{m}$  spacing with the cells in current clamp mode. To measure spontaneous miniature excitatory synaptic currents (mEPSCs) from L4 pyramidal neurons, the perfusate ACSF contains additional 1  $\mu\text{M}$  TTX and 10  $\mu\text{M}$  bicuculline. Whole cell recording was obtained in these neurons (voltage clamped at  $-70$  mV) using the same electrode internal solution as the LSPS experiments, and signals were acquired using the Digidata 1440A interface controlled by pClamp10.4 (Molecular Devices, Sunnyvale, CA).

### Visual Water Task

Visual acuity was estimated with the Visual Water Task [9, 10, 28]. In brief, two monitors were positioned at the wide end of a trapezoidal tank behind clear plexiglass. One monitor displayed a sinusoidal spatial frequency grating at 95% contrast, while the other displayed an isoluminant gray screen. The luminance of the two monitors was matched and gamma corrected with computer software (Eye-One Match 3). Inside the tank, the monitors were separated by a 46cm divider. The spatial frequency was determined relative to the length of this divider. The tank was filled with water and a hidden platform submerged below the surface of the water in front of the monitor displaying the grating.

Using a low spatial frequency (0.1 cycles per degree (cpd)), mice were trained to swim toward the monitor displaying the grating and hidden platform after a molding phase during which mice gradually learned to swim from a release chute at the back of the tank toward the monitors. During the training phase, when a mouse chose incorrectly, it repeated the trial on the same side until it chose correctly and was then returned to its home cage. For both the training, and the subsequent testing phase, mice swam blocks of 10 interleaved trials in groups of 5 for a maximum of 4 blocks of trials per day.

During the testing phase, the spatial frequency was increased in small, sequential increments until an animal consistently fell to 70% accuracy. Starting at 0.1 cpd, mice had to succeed at three consecutive trials before proceeding to the next spatial frequency, which presented one more complete cycle of the sinusoidal grating. Following the first failure, mice were required to achieve 5 correct trials in a row, or 8 correct trials out of 10 at each spatial frequency before proceeding to the next higher frequency. Once a mouse failed to complete 8 correct trials out of 10 at a given spatial frequency, it was briefly retrained at half that spatial frequency to eliminate any potential 'side bias'. Then, testing resumed at the spatial frequency below the original failure. The threshold for visual acuity was established once a mouse exhibited a consistent pattern of performance. Acuity thresholds were estimated as the spatial frequency average from three or more failures at adjacent spatial frequencies. Throughout the testing phase, any mouse that failed to find the hidden platform on the first try repeated the trial one more time before it was returned to its home cage, whether or not it chose correctly the second time.

### Tamoxifen Treatment

Tamoxifen was administered as previously described [17, 48]. In brief, tamoxifen (Sigma T5648) was solubilized in corn oil at 10mg/ml. A group of *ngr1(f/f);ER-Cre* and *ngr1(f/f)* mice was treated with tamoxifen for 3 consecutive days (100mg/kg i.p.) at P42. NgR1 protein is not detectable in *ngr1(f/f);ER-Cre* mice 7-14 after tamoxifen administration [17]. Upon completion of all experiments, immunoblots from brain tissue in primary visual cortex were performed to confirm that NgR1 protein expression was successfully abolished selectively in *ngr1(f/f);ER-Cre* mice, but not control *ngr1(f/f)* mice.

### Immunoblotting

Cortical punches (2mm diameter, 1mm thickness) were taken from visual cortex in both hemispheres and homogenized in 20 volumes of homogenization buffer (100mM Tris 7.4, 150mM NaCl, 5mM EDTA, 1mM DTT). Proteins were extracted from the homogenate by adding 1% SDS and 1% Triton X-100 followed by a 1 h incubation at 4°C on a nutator. Samples were then prepared for electrophoresis by adding protein loading buffer (20mM Tris pH6.8; 2% SDS; 10% glycerol; 2.5% beta-mercaptoethanol; 0.1% bromophenol blue) and heat at 95°C for 3 min before a brief spin to pellet insoluble debris. Proteins were separated by size by loading samples on a 4%–12% tris-glycine polyacrylamide gradient gel (Lifetech), and running SDS-PAGE as previously described [17].

Immunoblotting was performed to confirm evidence of recombination of the conditional *ngr1(f/f)* allele and presence or absence of NgR1 in *ngr1(f/f);ER-Cre* and *ngr1(f/f)* animals treated with tamoxifen. Blots were washed (3  $\times$  10 min) in PBS-T and incubated in blocking solution (3% BSA, 0.05% sodium azide, 0.1% Triton X) for 1 hr before a second series of washes (3  $\times$  10min TBST). First, blots were incubated in rabbit anti-GFP antibody (GeneTex, GTX26556) at 0.5 mg/ml for 1 h at room temperature. After repeated washing in PBS-T (3  $\times$  10 min), blots were incubated in HRP-conjugated secondary antibody (Jackson Immuno Research, 1:2000 in blocking solution) for 1 h at room temperature. After a final series of washes, immunoreaction was visualized with ECL (Pierce) and autoradiography film (Denville Scientific). Then, blots were incubated overnight at 4°C in blocking solution before being re-probed for NgR1 with goat anti-NgR1 antibody (R&D systems, AF1440) at 5  $\mu\text{g}/\text{ml}$  and HRP-conjugated secondary antibody 1:2000 in blocking solution.

### QUANTIFICATION AND STATISTICAL ANALYSIS

All statistical analyses were performed using Prism software (version 6.0, GraphPad). Groups numbers are stated in the Figure Legends.  $N$  represents number of mice for group comparisons and units for cumulative distributions, except for [Figures 2](#) and [3](#) where  $n$  corresponds to number of cells. Unless otherwise stated, group comparisons were made using unpaired non-parametric tests (Mann-Whitney test). Where multiple groups are compared, we applied the Kruskal-Wallis test with Dunn's multiple comparisons test. Error bars represent  $\pm$  sem.

### DATA AND SOFTWARE AVAILABILITY

No new software was generated in this study. MATLAB scripts for visual stimulus presentation and LSPS are published [[10](#), [57](#), [63](#)].